Contents lists available at ScienceDirect

High Energy Density Physics

journal homepage: www.elsevier.com

Ab initio simulations of liquid carbon monoxide at high pressure

Tanis C. Leonhardi [a, *], Burkhard Militzer [a, b]

[a] *Department of Earth and Planetary Science, University of California, Berkeley, California 94720, USA*
[b] *Department of Astronomy, University of California, Berkeley, California 94720, USA*

ARTICLE INFO

Article history:
Received 1 September 2016
Accepted 10 February 2017
Available online xxx

Keywords:
Carbon monoxide
Density functional theory
First principles molecular dynamics
Equation of state
Planetary interiors

ABSTRACT

Carbon monoxide occurs as a volatile species in the interiors of terrestrial planets, and as a disequilibrium atmospheric constituent in the giant planets. It plays an important role during the accretionary stages of planet formation reacting with gases to form compounds such as CH_4 and H_2O. The structure of carbon monoxide is unknown over the majority of the temperature and pressure regime in giant planet interiors. Here we perform *ab initio* molecular dynamics simulations to characterize CO to 140 GPa and 5,000 K. We find that CO is stable as a molecular liquid at lower P-T conditions, as a polymeric liquid at higher P-T conditions found in ice giant interiors, and as a plasma at high-T.

1. Introduction

Carbon monoxide ice is one of the solid phases accreted during the formation of ice giant planets alongside other organic (C, N, O, H)-rich ices and dust grains [1–3]. These ice particles react with gases, dust, and other ices present during, and after, planetary accretion to form compounds, including CH_4 and H_2O, which are commonly observed in giant planet atmospheres today [1–6]. A recent study developed a 'volatile distribution model' in which chemical and physical dynamics of the protoplanetary disk are incorporated with an accretionary planet formation model for Uranus and Neptune to explain observed trace element and isotopic compositional differences between these two planets [3]. Thus understanding the structure and behavior of CO at the temperatures and pressures of giant planet interiors is important for understanding the physical conditions during the first stages of giant planet formation and evolution.

Determining the structure, stability, and properties of planetary ices composed of C—H—O—N compounds at high temperatures and pressures can also help in understanding magnetic field generation in ice giant planets. For example, knowing the phase and transport properties of the ices would be particularly useful in assessing one proposed model of Uranus' and Neptune' magnetic field generation in which convection in layers of ices with low conductivity generate the planets' observed field [7–12]. It is important to point out that here 'ice' refers to the material's state during planet formation, now these materials may exist in liquid or superionic form in the hot interiors of giant planets [13].

Despite the relatively high abundance of C and O in the ice giants, only one experimental study has explored the stability and properties of CO at GPa pressure [14]. In the study, Nellis et al. [14] used a combination of experiments and numerical calculations to determine the shock Hugoniot curve of liquid CO from 5 to 60 GPa. This means the structure and properties of CO remain unknown over the majority of the P-T regime inside Neptune's and Uranus's ice layer (reaching up 7000 K and 600 GPa) [15,16]. Determining the structure of CO over P-T conditions inside giant planets is important for improving our understanding of the current structure of ice giants and their formation processes.

In this study we use first-principles molecular dynamics simulations based on density functional theory [17] to construct a P-T phase diagram for liquid CO up to 140 GPa and 5000 K. Results from these simulations were used to study the structure of liquid CO and provide a first constraint on the melting line of CO at high temperatures and pressures. We compare our results with previous experimental results and one predicted isentrope for Uranus's ice layer [15].

2. Computational methods

First-principles molecular dynamics (FPMD) simulations based on density functional theory (DFT) [17] were performed using the Vienna *ab initio* Simulation Package (VASP) [18]. These simulations used the generalized gradient approximation (GGA) with a Perdew-Burke-Ernzerhof exchange-correlation functional [19] and projector augmented wave (PAW) pseudopotentials [20]. The Brillouin zone was sampled using Γ point only. An energy cut-off value of 1000 eV was used to represent the electronic orbital in a plane-wave basis as it provided convergence of pressures and energies to less than 1% uncertainty.

All simulations were performed with periodic boundary conditions and temperatures were kept constant by a Nosé-Hoover thermostat [21,22]. Previous FPMD simulations of CO_2 showed that results

* Corresponding author.
Email address: tcleonhardi@berkeley.edu (T.C. Leonhardi)

http://dx.doi.org/10.1016/j.hedp.2017.02.005
1574-1818/

are converged with 32 molecules (96 atoms) in the simulation cell [23,24]. Hence we used a 3 × 3 × 3 body centered cubic supercell of 54 CO molecules (108 atoms) to mitigate finite size effects. Simulations were run with a 1.0 fs time step and total simulation time varied between 2 and 12 ps in length depending on the system temperature. At higher temperatures, equilibrium is obtained faster, so shorter simulation times can be performed.

Simulations systematically sampled a NVT ensemble (N = # particles, V = Volume, T = Temperature) up to 140 GPa and 5000 K. An additional simulation with a density of 0.82 g/cc was performed at 9000 K to evaluate the extent of CO dissociation into C and O atoms and study a CO plasma. The trajectory for each of these simulations was used to determine the atomic coordination of C atoms. Here we use the terminology employed in previous studies [23,24] to define the carbon coordination as the number of oxygen and carbon atoms within a specified radial cut-off distance of a given carbon atom. The cut-off distance used for coordination determination was the first minimum of the C—O pair correlation function, see for example Boates et al. [23].

3. Results and discussion

The CO phases observed from each simulation were mapped onto a high pressure, high temperature phase diagram (Fig. 1). Calculated pressures and energies for these simulations are reported in Table 1. For the purpose of defining phase boundaries we used a molecular fraction cutoff of 0.5. This means that the molecular liquid contained ≥ 50% CO molecules. Molecules with C—C bonds were classified as C—C polymers. Visualizations of the observed liquid phases and a partially dissociated phase are provided in Fig. 2.

3.1. Liquid phases

At low temperatures and pressures we observed CO as a molecular liquid. Abundant CO molecules produced CO pair correlation functions with a peak at the characteristic distance of 1.128 Å (see Fig. 3), which corresponds to the C—O triple bond length [25]. As we increased the density, the coordination of carbon atoms increased from 1 to 2, thus becoming more polymerized. The higher C coordination corresponded to the development of CO_2 molecules and polymers with C—C bonds, visualized in Fig. 2B. In our phase diagram, polymeric liquid refers to a liquid consisting of C—C polymers and CO_2 molecules. These new polymers were observed indirectly as a drop in the peak value of the C—O pair correlation function, the development of a C—C peak at 1.38 Å, and a O—O peak at 2.32 Å (Fig. 3). The O—O distribution peak distance has the same value as the distance between oxygen nuclei bound in a CO_2 molecule [26]. Single C—C bonds have an interatomic distance of 1.54 Å, double C—C bonds of 1.34 Å, and triple C—C triple of 1.2 Å [27]. The observed distance of 1.38 Å for the C—C pair correlation function is characteristic of double C—C bonds. However additional work investigating the details of C—C bonding needs to be performed to characterize the nature of C—C bonds in the polymers observed in Figs. 2B and 3B.

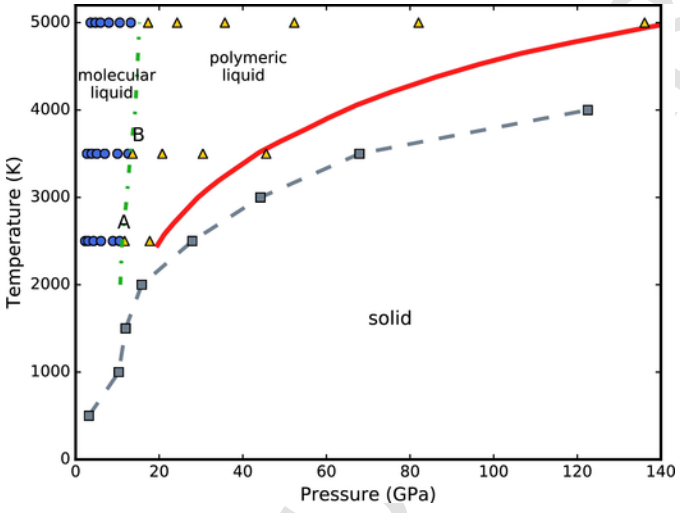

Fig. 1. Preliminary P-T phase diagram of CO based on phases observed in performed simulations. The green dashed-dotted line represents the transition between majority molecular carbon and majority 2-coordinated (polymeric) carbon. Squares mark melting points determined through single-phase isothermal compression simulations, the dashed line thus represents a lower bound of the true melting line. The red solid line represents an isentrope calculated for Uranus's ice layer [14]. Results from simulations marked as A and B are shown in Fig. 2 and Fig. 3.

Table 1.
Pressure and internal energy from our FPMD simulations along three isotherms. Parentheses denote 1 σ error bars.

T (K)	ρ (g/cc)	P (GPa)	E (eV/CO)
2500[A]	0.823	2.30(2)	−0.51482(7)
3500	0.823	2.73(2)	−0.50049(8)
5000	0.823	3.61(3)	−0.4825(2)
9000[C]	0.823	4.37(6)	−0.391(4)
2500	0.954	2.99(2)	−0.51061(8)
3500	0.954	3.82(3)	−0.4990(2)
5000	0.954	4.77(2)	−0.4788(3)
2500	1.106	4.28(3)	−0.50783(9)
3500	1.106	5.09(3)	−0.4963(4)
5000	1.106	5.96(5)	−0.4734(4)
2500	1.283	6.06(4)	−0.5032(1)
3500	1.283	6.98(6)	−0.4908(2)
5000	1.283	7.96(7)	−0.4674(4)
2500	1.487	8.927(87)	−0.5066(3)
3500	1.487	10.02(9)	−0.4865(2)
5000	1.487	10.56(10)	−0.4652(6)
2500	1.725	10.54(6)	−0.5084(3)
3500	1.725	12.62(9)	−0.4853(4)
5000	1.725	13.19(13)	−0.4594(5)
2500	2.000	11.74(10)	−0.5137(8)
3500[B]	2.000	13.63(8)	−0.4982(6)
5000	2.000	17.34(17)	−0.4540(6)
2500	2.319	17.74(17)	−0.5081(5)
3500	2.319	20.74(19)	−0.4891(3)
5000	2.319	24.30(24)	−0.4427(6)
3500	2.689	30.45(22)	−0.4746(7)
5000	2.689	35.70(23)	−0.4332(7)
3500	3.118	45.59(31)	−0.4644(6)
5000	3.118	52.31(37)	−0.4181(5)
5000	3.616	82.03(43)	−0.4000(8)
5000	4.193	136.11(46)	−0.3742(6)

[A,B,C] Pair correlation functions and snapshots from these simulations are provided in Fig. 3 and Fig. 2 respectively.

In addition to analyzing the peaks in the pair correlation functions, we also performed a cluster analysis for the polymeric simulation 'B'. Two atoms were considered to be part of the same cluster if they are separated by less than 1.90 Å. Based on this simple geometric criterion, we determined the clusters for every configuration and then averaged the results along the trajectory. Zero O_2 molecules were found in the entire simulation, which implies the C—O bonding is strong and a sufficient number of carbon atoms were present to prevent the formation of O_2 molecules.

Our analysis also revealed that CO_2, CO, and C_2O_3 clusters occurred most frequently. However, they contained only 28.4%, 6.7% and 4.6% of the C atoms, respectively. The majority of the C atoms, 57.6%, were stored long C—O polymers that contained at least 21 C and 8 O atoms. On average, these polymers consisted of 31.1 C and

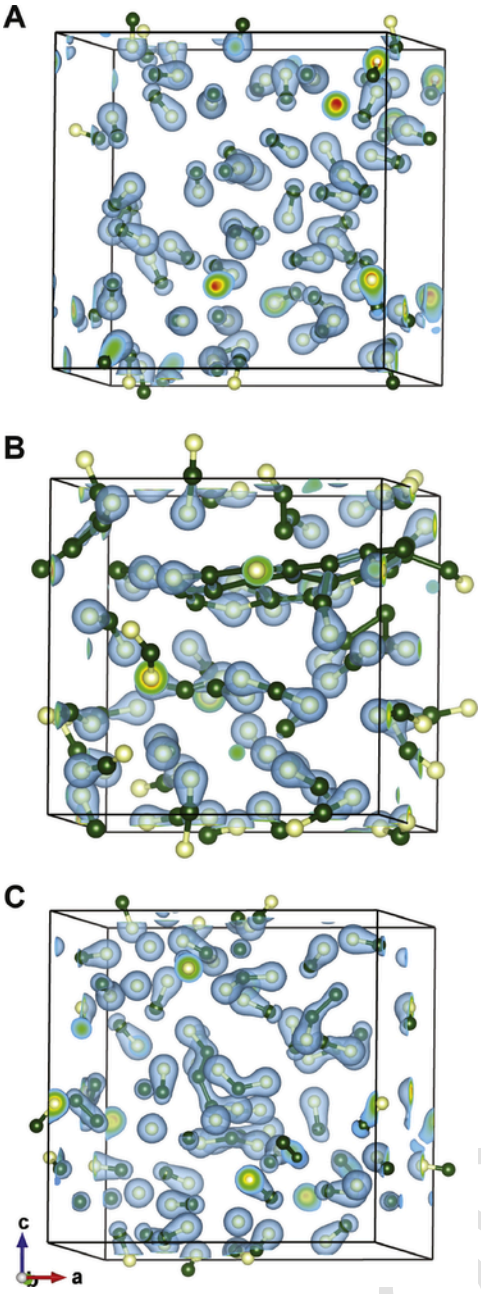

Fig. 2. Molecular dynamics snapshots showing three observed structures of CO: (A) molecular liquid at 2500 K and 0.82 g/cc (2.30 GPa), (B) polymeric liquid at 3500 K and 2.00 g/cc (13.63 GPa), and (C) partially dissociated molecular liquid at 9000 K and 0.82 g/cc (4.37 GPa). The corresponding pair correlation functions are shown in Fig. 3. Carbon and oxygen atoms are depicted by the green and white spheres respectively. The blue isosurface shows the density of the valence electrons.

16.0 O atoms, which implies that a C:O ratio of 2:1 is particularly favorable. We can thus write the following approximate polymerization reaction,

$$3n\,CO \rightarrow n\,CO_2 + \left[C_{2n}O_n\right]_{polymer},$$

while keeping in mind that a variety of polymers with $n \geq 21$ were produced. A small remainder of 2.7% C atoms were found to occur in small short-lived clusters with up to 6 C atoms.

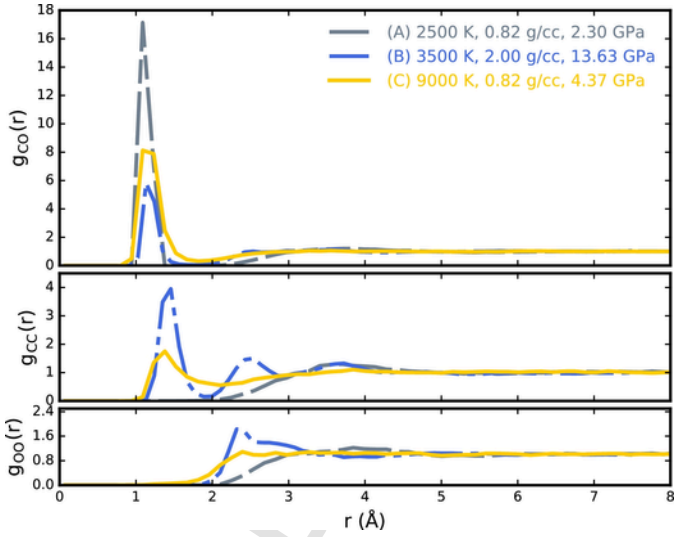

Fig. 3. Pair correlation functions for simulations showing three different structures. (A) molecular liquid, (B) polymeric liquid, (C) partially dissociated liquid. Here A, B, and C refer to the same simulations whose snapshots are shown in Fig. 2 and plotted in Fig. 1.

The transition from a molecular to a polymeric liquid is associated with a decrease in slope of the P-V curve at fixed T shown in Fig. 4. This change in slope is more distinct when plotted as a P*V vs. V curve in Fig. 4. Molecular dynamics studies of N_2 [28], H_2 [29], and CO_2 [24] found that a plateau in the P-V equation of state for those systems corresponded to a first order liquid-liquid phase transition (LLPT). Boates et al. determined that the CO_2 first-order LLPT corresponded to a rapid decrease in the 2-coordination of C, increase in C 3-coordination, and the formation of stable CO_3 molecules [24]. Beyond the LLPT at much higher temperatures and pressures, carbon gradually transition from 3-coordination to short-lived 4-coordination species. The plateau in the CO P-V curve observed in this study may correspond to a first order LLPT similar to that observed for CO_2,

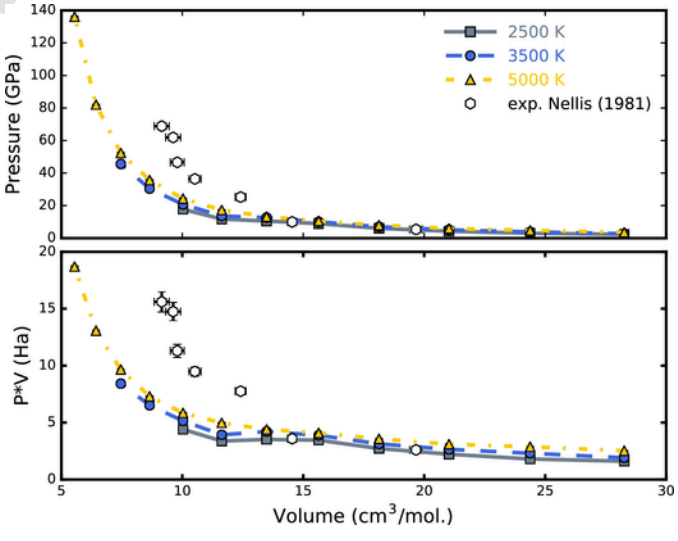

Fig. 4. P-V equation of state along three isotherms plotted along with calculated and experimentally derived points on the CO shock Hugoniot curve [13]. The decrease in slope of the P-V curve ≤ 3500 K is more distinct when plotted as a P*V vs. V curve. Only the two lowest pressure experimental data points correlate to temperatures sampled in this study.

where the molecular liquid becomes a polymeric liquid. However, with the results from this study we cannot conclusively state whether there is an LLPT between molecular and polymeric CO. Additional work sampling P-T space with a finer grid could provide insight on this matter.

3.2. CO dissociation

Only one experimental study has explored the structure of CO at high temperatures and pressures. This study by Nellis et al. (1981) [14] used gas-gun shock experiments to determine the CO Hugoniot curve up to 60 GPa. Their P-V results are plotted alongside our results in Fig. 4. For the low pressure (≤ 10 GPa) experimental data points, our results suggest a shock temperature between 2000 K and 3000 K, which is in agreements with temperature predictions for these shock pressures which spanned 2000 to 3000 K [14]. These experiments reported a rapid change in slope of the P-V line above 10 GPa [14]. The high pressure (≥ 10 GPa) data points did not fall along the predicted CO shock Hugoniot curve and were explained by the presence of high density carbon phases, primarily diamond [14]. Temperatures were predicted at 7000 K for the 30 GPa data point and > 10,000 K for the 50–60 GPa data points. The P-T space sampled in our study only extended to 5000 K in the ≥ 30 GPa range, so we cannot evaluate the state of the system at the higher pressure experimental data points.

Nellis et al. interpreted the CO shock measurements as representing dissociation of CO molecules into diamond, ± graphite, CO_2, and O_2 above 10 GPa, resulting in a change of slope in the P-V equation of state [14]. The researchers proposed complete dissolution of CO into diamond occurs by 30 GPa and 7000 K [14]. Over the 10–30 GPa pressure range and 3000–7000 K they inferred that CO dissociated into CO_2, diamond, and O_2, although these phases were not directly observed co-existing.

Simulations performed along isotherms up to 3500 K showed plateaus in the P-V slope (Fig. 4). By 5000 K there was no observable drop in pressure along the P-V curve, suggesting that a LLPT does not exist at high-T. Evidence of dissociation in the 4000–5000 K simulations was also observed as broadening of pair correlation function peaks and infilling of distribution minima. If O_2 formed in a simulation, as is predicted from experimental studies [14] we would expect to see a peak at 1.208 Å [30] in the O—O pair correlation function, a peak at 1.54 in the C—C distribution for the single C—C bond, and a peak at 2.32 Å for the interatomic distance between oxygen atoms bound in CO_2 Å [26]. We observed no such O—O peak, suggesting O_2 was not produced in our simulations. The only observed peak in the O—O pair correlation function for our simulations was a peak at 2.32 Å, from which we conclude CO_2 was formed. A peak in the C—C distribution at 1.38 Å was common to many simulations, however this does not correspond to the characteristic length of the single C—C bond in diamond. These results suggest that CO_2 formed, O_2 did not, and C formed polymers with C—C bonds rather than diamond or graphite. However, the increased polymerization of C to form CO_2 molecules was observed in our simulations as was predicted by previous experimental results [14].

We performed one additional simulation with a density of 0.82 g/cc at 9000 K to see if full CO dissociation was achieved by 9000 K. The pair correlation functions for this simulation are plotted in Fig. 3. For complete dissociation we expect complete infilling of minima and broadening of maxima to form one smooth distribution. While infilling and broadening are clearly evident in the 9000 K simulation, there are still pronounced maxima for the C—O and C—C correlation distributions. Molecules with short-lived (< 15 fs) C—C bonds were observed in these simulations. These results show a similar behavior to CH_4 [31] and a bulk C:H:O:N liquid [32] which also developed molecules with short-lived C—C bonds at high temperatures. Our results suggest that complete dissociation of CO has not occurred at 9000 K and low pressures. Additional simulations up to and above 10,000 K at higher pressures can constrain the conditions necessary for full dissociation of CO.

3.3. Melting line and implications for giant planet interiors

We used isothermal single-phase compression simulations to determine the CO melting line. These simulations may experience supercooling as they are compressed. Our simulations froze into an amorphous structure. We assume an ordered CO solid may be more stable. We also did not reverse this transformation by expanding our frozen simulations. For these reasons, we expect our proposed melting line to be a lower bound in P-T space for the true CO melting line.

The first completely frozen simulation was designated the melting point for a given isotherm. We plotted the resulting melting line along with an isentrope for the temperatures and pressures inside Uranus's ice layer in Fig. 1. Our findings predict that CO would exist as a polymeric liquid in Uranus's ice layer. Numerical models of magnetic field generation field on Uranus and Neptune compared with observational information about their magnetic favor dynamo generation in a layer of convecting liquid characterized by poor conductivity [10–12]. Recent findings show that the development of C—C bonds in H—O—C—N liquids greatly affects their conductivity and viscosity, which in turn impacts the magnetic Reynolds number and the nature of a magnetic field generated by the liquid [32]. The development of C—C in our simulations potentially correlates to changes in CO properties. Additional work determining the conductivities and transport properties of CO across the full P-T regime inside these planets would be useful in determining if CO may be an ice contributing to magnetic field generation.

4. Conclusions and implications

The phase diagram constructed in this study is the first P-T phase diagram for CO extending to 140 GPa and 5000 K. We found that carbon existed in 1-coordination in CO molecules as a molecular liquid at low temperatures and pressures. Between 8–13 GPa we observed a transition from a molecular liquid to a polymeric liquid. Additional work constraining the conditions of this transition will allow for determination of whether it is a gradual change or an abrupt change that corresponds to a first order liquid-liquid phase transition. Our proposed phase diagram suggests that CO may exist as a polymeric liquid in Uranus's ice layer.

Acknowledgments

This work was supported in part by NSF and by the U.S. Department of Energy (DOE) grants DE-SC0010517 and DE-SC0016248. Computational resources were provided by the National Energy Research Scientific Computing Center (NERSC).

References

1. R.G. Prinn, B. Fegley Jr., Kinetic inhibition of CO and N_2 reduction in circumplanetary nebulae: implications for satellite composition, Astrophys. J. 249 (1981) 308–317.
2. G.P. Horedt, W.B. Hubbard, Two and three layer models of Uranus, Moon Planets 29 (3) (1983) 229–236.
3. M. Ali-Dib, O. Mousis, J-M. Petit, J.I. Lunine, The measured compositions of Uranus and Neptune from their formation on the CO ice line, Astrophys. J. 793 (2014) 9.

4. A. Marten, D. Gautier, T. Owen, D.B. Sanders, H.E. Matthews, S.K. Atreya, First observations of CO and HCN on Neptune and Uranus at millimeter wavelengths and the implications for atmospheric chemistry, Astrophys. J. 406 (1993) 285–297.
5. K. Lodders, B. Fegley Jr., Atmospheric chemistry in giant planets, brown dwarfs, and low-mass dwarf stars, Icarus 155 (2) (2012) 393–424.
6. T. Encrenaz, E. Lellouch, P. Drossart, H. Feuchtgruber, G.S. Orton, S.K. Atreya, The detection of carbon monoxide in the atmosphere of Uranus, EOS 115 (35-36) (2004) 35–36.
7. W.J. Nellis, D.C. Hamilton, N.C. Holmes, H.B. Radousky, F.H. Ree, A.C. Mitchell, M. Nicol, The nature of the interior of Uranus based on studies of planetary ices at high dynamic pressure, Science 240 (4853) (1988) 779–781.
8. J.E.P. Connerey, M.H. Acuña, N.F. Hess, The magnetic field of neptune, J. Geophys. Res. 96 (1991) 19023–19042.
9. J.E.P Connerey, Magnetic fields of the outer planets, J. Geophys. Res. 98 (E10) (1993) 18659–18679.
10. S. Stanley, J. Bloxham, Convective-region geometry as the cause of Uranus' and Neptune's unusual magnetic fields, Nature 428 (151-153) (2004) 151–153.
11. S. Stanley, J. Bloxham, Numerical dynamo models of Uranus' and Neptune's magnetic fields, Icarus 184 (2) (2006) 556–572.
12. S. Stanley, G.A. Glatzmaier, Dynamo models for planets other than earth, Space Sci. Rev. 1 (2009) 1.
13. H.F. Wilson, M.L. Wong, B. Militzer, Superionic phase change in water: consequences for the interiors of Uranus and Neptune, Phys. Rev. Lett. 110 (2013), 151102.
14. W.J. Nellis, F.H. Ree, M. van Thiel, A.C. Mitchell, Shock compression of liquid carbon monoxide and methane to 90 GPa (900 kbar), J. Chem Phys. 75 (6) (1988) 3055–3063.
15. M. Ross, The ice layer in Uranus and Neptune-diamonds in the sky?, Nature 292 (435-436) (1981) 435–436.
16. N. Nettelmann, R. Helled, J.J. Fortney, R. Redmer, New indication for a dichotomy in the interior structure of Uranus and Neptune from the application of modified shape and rotation, Planet. Space Sci. 77 (2013) 143–151.
17. P. Hohenberg, W. Kohn, Inhomogeneous Electron Gas, Phys. Rev. 136 (3B) (1964) B864.
18. G. Kress, J. Furthmüller, Efficient iterative schemes for ab initio total-energy calculations using a plane-wave basis set, Phys. Rev. B 54 (1996) 11169.
19. J.P. Perdew, K. Burke, M. Ernzerhof, Generalized gradient approximation made simple, Phys. Rev. Lett. 77 (1996) 3865.
20. P.E. Blochl, Projector augmented-wave method, Phys. Rev. B 50 (1994) 17953.
21. S. Nosé, A unified formulation of the constant temperature molecular dynamics method, J. Chem. Phys. 81 (1) (1984) 511–519.
22. S. Nosé, Constant Temperature Molecular Dynamics Methods, Prog. Theor. Phys. Suppl. 103 (1991) 1–46.
23. B. Boates, S. Hamel, E. Schwegler, S.A. Bonev, Structural and optical properties of liquid CO_2 for pressures up to 1 TPa, J. Chem. Phys. 134 (2011), 064504.
24. B. Boates, A.M. Teweldeberhan, S.A. Bonev, Stability of dense liquid carbon dioxide, PNAS 109 (37) (2012) 14808–14812.
25. F.J. Lovas, E. Tiemann, J.S. Coursey, S.A. Kotochigova, J. Chang, K. Olsen, R.A. Dragoset, NIST Diatomic Spectral Database (2002), http://www.nist.gov/pml/data/msd-di/index.cfm.
26. G. Herzberg, Electronic Spectra and Electronic Structure of Polyatomic Molecules, Van Nostrand, New York, 1966.
27. K. Kuchitsu (Ed.), Structure of Free Polyatomic Molecules - Basic Data, Springer-Verlag, Berlin, 1998.
28. B. Boates, S.A. Bonev, First-order liquid–liquid phase transition in compressed nitrogen, Phys. Rev. Lett. 102 (2009), 015701.
29. M.A. Morales, C. Pierleoni, E. Schwegler, D.M. Ceperley, Evidence for a first-order liquid-liquid transition in high pressure hydrogen from ab initio simulations, PNAS 107 (29) (2010) 12799–12803.
30. K.P. Huber, G. Herzberg, Molecular spectra and molecular structure. IV, Constants of Diatomic Molecules, Van Nostrand Reinhold Co., New York, 1979.
31. B.L. Sherman, H.F. Wilson, D. Weeraratne, B. Militzer, Ab inition simulations of hot, dense methane during shock experiments, Phys. Rev. B 86 (2012), 224113.
32. R. Chau, S. Hamel, W.J. Nellis, Chemical processes in the deep interior of Uranus, Nat. Commun. 2 (2011) 203.